Mission Analysis and Navigation Design for Uranus Atmospheric Flight

Bessette, Emilie; Mooij, E.; Stam, D.M.

DOI
10.2514/6.2022-0250

Publication date
2022

Document Version
Final published version

Published in
AIAA SCITECH 2022 Forum

AIAA SciTech Forum
January 3-7, 2022, San Diego, CA & Virtual
AIAA SCITECH 2022 Forum

10.2514/6.2022-0250

Mission Analysis and Navigation Design for Uranus Atmospheric Flight

E. Bessette*, E. Mooij† and D.M. Stam‡
Faculty of Aerospace Engineering, Delft University of Technology, Kluyverweg 1, 2629 HS Delft, The Netherlands

We present a 3 Degrees of Freedom mission design and analysis for in-situ probing of Uranus' atmosphere consisting of two un-propelled gliders and one orbiting spacecraft in continuous line of sight. We focus on the study of the gliders' navigation and science modules. Because of the lack of a Global Navigation Satellite System around Uranus and the ineffective use of optical sensors due to the planet's large distance to the Sun and high atmospheric opacity, the post-processing relation between the vehicles' estimated state and measured scientific data is investigated to yield accurate state estimations. In-situ probing by the two gliders will make it possible to measure spatially variable atmospheric properties over a flight duration of up to 12 Earth days, as compared to a few hours for a conventional descent probe. Future work will include a 6 Degrees of Freedom simulation of the vehicles' flight, the chosen planet's wind model, a Flush Air Data Sensor as an additional navigation sensor, and a band-pass filter to reduce the estimated variables' noise.

Nomenclature

A, B, C	=	material resistance constants, K^{-1}	s	=	accelerometer scale factor, -
a	=	acceleration, m/s^2	T	=	temperature, K
b	=	accelerometer bias, m/s^2	t	=	time, s
C_D, C_L	=	drag and lift coefficient, -	V	=	velocity, m/s
c	=	speed of light, m/s	W/S	=	aircraft wing loading, N/m^2
f	=	frequency, Hz	α	=	angle of attack, rad
m	=	mass, kg	λ	=	latitude, rad
m	=	accelerometer misalignment, -	ρ	=	density, kg/m^3
R_T	=	resistance at temperature T, Ω	$\tilde{\rho}$	=	pseudo range, m
$R_{u,e}$	=	Uranus equatorial radius, m	$\dot{\tilde{\rho}}$	=	pseudo range rate, m/s
$\mathbf{r}$	=	position vector, m	σ	=	standard deviation, -
$\dot{\mathbf{r}}$	=	velocity vector, m/s	τ	=	longitude, rad
S_{ref}	=	vehicle reference area, m^2			

I. Introduction

Voyager 2 was the first and only spacecraft to visit Uranus and Neptune in 1986 and 1989, respectively. Since then, all Ice Giants' studies have been performed with ground-based and space telescopes in Earth orbits. No spacecraft has ever performed in-situ measurements of either of these planets. Thanks to a fortuitous alignment of the Solar System's planets, the 2030s will offer this possibility, as gravity assists of both Venus and Jupiter, combined with the illumination of Uranus' and Neptune's hemispheres unobservable to Voyager will allow for a smaller fuel consumption and new science opportunities respectively. NASA and ESA have worked independently and collaboratively to define elements essential to such a mission: science priorities, mission concepts with potential architectures, promising science payload to fulfil the science objectives, and science return potential in studying Uranus and Neptune [1–5]. The main conclusions from these studies are that Uranus and Neptune are considered equally valuable to explore, and that there is a need for an atmospheric vehicle in a mission's architecture. The highest priority science objectives were specified as

*MSc Student, section Astrodynamics and Space Missions, bessette@student.tudelft.nl.
†Associate Professor, section Astrodynamics and Space Missions, e.mooij@tudelft.nl, Associate Fellow AIAA.
‡Associate Professor, section Astrodynamics and Space Missions, d.m.stam@tudelft.nl

measuring abundances of noble gases and their isotopes, pressure, temperature, and density profiles, and abundances of heavier elements and disequilibrium species. The latter measurements require much deeper probing of the atmospheres.

In-situ knowledge of an Ice Giant's atmosphere can provide information on the planet's formation and on that of the Solar System as a whole. In particular, it could provide insight into why several models predict the formation of these planets to be much closer to the Sun than where they presently are [6–11]. The following research question will drive this paper's study: How can knowledge about Uranus' current atmosphere help us understand the formation of the Ice Giants, and in a broader sense, that of the Solar System?

Most mission studies to the Ice Giants recommend the use of a mission architecture comprising of a parachuted descent probe and a relay spacecraft, to measure and transmit the scientific data back to Earth. This architecture has been proven to be safe and efficient, through the heritage of the Galileo mission to Jupiter and the Cassini-Huygens mission to Saturn and Titan. This study, however, will investigate the feasibility of conducting this class of mission with another type of craft, namely two gliders that explore Uranus' atmosphere in-situ. The focus will be on the systems' navigation filter, and on the post-processing relation between their estimated state and in-situ measured scientific data. All chosen navigation sensors and scientific instruments related to navigation will be modelled and coupled with a 3 Degrees of Freedom (DoF) flight dynamics model to prove that the gliders' state can be estimated accurately, and that the mission can be flown in a controlled manner. Scientific instruments are used as navigation sensors to tackle the absence of Global Navigation Satellite System (GNSS) satellites and the ineffective use of optical sensors due to Uranus' large distance to the Sun and high-opacity atmosphere. The navigation module shall provide accurate information on the gliders' estimated state, and on any other knowledge needed to interpret the measured scientific data. Modelling of the sensors will be restricted to those relevant to the navigation system. In addition, no wind model is considered, although it will be integrated in future work.

The layout of this paper is as follows. In Sec. II an overview of the proposed method is given, including a motivation for the choice of target planet, the mission's scientific aim and choice for target areas to probe, the chosen platform, and its scientific payload. The orbiter's launch and interplanetary trajectory parameters, as well as orbital parameters at Uranus are mentioned, the software used and GNC configuration are introduced, and the navigation and science aspects are documented. In Sec. III we present the results related to estimates of the vehicles' state and auxiliary parameters used for post-processing the science data. Section IV, finally, provides concluding remarks on the work performed and gives an outlook of the ongoing work.

II. Proposed Method

The proposed mission architecture consists of a spacecraft orbiting Uranus in a circular orbit, in continuous line of sight of two gliders flying in symmetrical flights, at different latitudes.

A. Choice of Planet

Uranus was the preferred candidate for this study because its atmosphere appears to be less active and thus less prone to destabilise a vehicle with strong winds. Indeed, Uranus was observed to be much quieter than Neptune, showing less cloud activity and infrequent storms [12]. Moreover, it is closer to Earth than Neptune, which means that the mission's costs would be reduced due to a shorter travel time and most probably a lighter craft. The planet's gravity was modelled as a central field as other perturbations (solar radiation pressure, planetary albedo, planetary radiation pressure, thermal radiation, antenna thrust, and gravitational attraction of the Sun and other Solar System planets) were determined to be negligible. For the atmospheric density, the model described in Helled et al. [13] was implemented. The temperature-pressure profiles were modelled and extrapolated from the data given by Lindal [14] as derived from the Voyager 2 radio occultation measurements. Although not used in the work presented here, the planet's zonal wind model is modelled following Hammel et al. [15].

B. Scientific Aim and Choice of Target Areas

With all known properties of Uranus and Neptune having been obtained from fly-by spacecraft observations, and ground-based or space-based telescopes, the need for in-situ knowledge is all the more important. Remote-sensing cannot provide a complete picture of a planet's atmospheric parameters, dynamics, and interiors, and is ultimately constrained by multiple elements such as the limited penetration depth of solar visible and thermal radiation, degeneracies between the effects of temperatures, clouds, hazes, and gas abundances on the emergent spectra, as well as the essential fact that some key atmospheric constituents cannot be detected remotely [16]. The formation of the Ice Giants is predicted to

have taken place much closer to the Sun than where these planets presently are [6–11]. To help tackle such a knowledge gap, in-situ knowledge on Uranus' atmosphere could be extrapolated to the planet's formation and thus to the formation of Ice Giants and consequently of the Solar System.

As a priority in this mission, it is hence decided to focus on the in-situ study of Uranus' atmosphere. The science objectives of a mission to one of the Ice Giants can be divided into three categories: Tier 1, Tier 2A, and Tier 2B, in order of decreasing importance [16]. Tier 1 and Tier 2A science objectives can be performed with the same instruments and consist in measuring atmospheric constituents well beneath the tropopause. Tier 2B science objectives require an even deeper probing and are much more sensitive to the local weather, and thus to the entry and descent location and time. To yield a more complete measurement dataset, it is interesting to probe layers of the atmosphere that are dominated by solar insolation, and layers that are beyond the reach of the Sun's direct influence, as well as the transition region between the two. Moreover, exploring the planets' northern hemisphere, as opposed to the southern hemisphere observed by Voyager 2, would undoubtedly yield new science data.

To achieve the science objectives mentioned by Atkinson et al. [16], we target Uranus' tropospheric region, which extends from 1 bar (0 km altitude) to 100 bar (-375 km altitude). The target latitudes and longitudes depend on both the planet's Summer/Winter arrangement at arrival, and on its wind patterns. Two types of zones have to be avoided: the ones with high zonal winds, and the ones where a transition between prograde and retrograde winds occur, as they might more easily destabilise the vehicles. The mission's target latitudes and longitudes were chosen by focusing on the science return they can offer and on their wind speeds:

- Equatorial Domain: This area is less challenging in terms of zonal winds. The deep atmosphere is enriched in CH_4 and H_2S, and possibly other volatiles such as NH_3 and H_2O due to rising motions from the 100 bar level or deeper. It is safer to remain between 0°-18.5° N to avoid the prograde/retrograde wind shift occurring at 18.5° N. However, the atmospheric vehicles should not probe too close to the equator, as a local minimum in upper tropospheric volatiles species is suspected there. An off-equatorial entry site is thus optimal, however the storm bands and strong up-welling of mid-latitudes [17] should also be avoided. The zonal wind velocity was calculated for different values of latitude close to the 18.5°N limit. It was decided to keep a 1° separation between the wind-shifting 18.5° latitude and the target latitude to minimise the zonal winds as much as possible. We therefore chose an equatorial latitude of 17.5°N, where the zonal wind is equal to -6.21 m/s.
- Polar Domain: The polar domain enables the measurement of noble gases and small-scale convective activity leading to potentially enhanced H_2 humidity immediately above the clouds. In order to encounter minimal zonal winds without being exactly on top of the planet's north pole, a separation of 1° was again taken between the limit and target latitude. This led to a polar target latitude of 89°N, where the zonal wind is of about 10.67 m/s.

Two atmospheric vehicles are thus needed to explore these two domains, with the equatorial one flying in retrograde direction, and the polar one flying in prograde direction to always experience tailwind. Uranus' northern hemisphere is visible before the planet's Spring solstice, which will take place in 2049. A launch on May 25, 2031 can bring the spacecraft to Uranus in 12 years, arriving on May 17, 2043 [1]. To explore both the day/Summer and night/Winter sides of Uranus at arrival, the polar glider will find itself on the day side of the planet. The equatorial glider will be placed on the night side of the planet, at longitudes higher than 10.5°, where the day/night terminator will be, as seen in Fig. 1.

C. Scientific Payload

Inspired by Atkinson et al. [16], our Tier 1 and Tier 2A instruments include: a Mass Spectrometer, a Tunable Laser Spectrometer, a Helium Abundance Detector, and an Atmospheric Structure Instrument, which contains an accelerometer and sensors for atmospheric pressure and temperature profile measurements used to derive the speed of sound. This speed of sound data are used to determine the ortho- to para-hydrogen ratios, which helps the interpretation of the atmosphere's properties such as its thermal profile and density structure. A NanoChem instrument is added to this Tier 1A instrument suite. Introduced by Sayanagi et al. [18], it consists of a set of carbon nanotube-based sensing elements, a pressure sensor, and a temperature sensor [19, 20]. It has demonstrated sensitivities to molecules such as CH_4, NH_3, H_2S. As mentioned before, Tier 2B instruments operate at lower altitudes than Tier 1 and 2A ones. They include the following instruments: a Nephelometer, a Net Flux Radiometer, and an Ultra High Frequency (UHF) Transceiver. The latter will be used for the Doppler wind experiment using the relay spacecraft's radio subsystem. All these instruments will be onboard the gliders, with the addition of radio transmitters and receivers on the orbiter for the Doppler wind experiment. The mission's science traceability matrix is shown in Table 5 and summarises how each scientific instrument helps to answer this study's research question, for a total payload mass of approximately 25 kg.

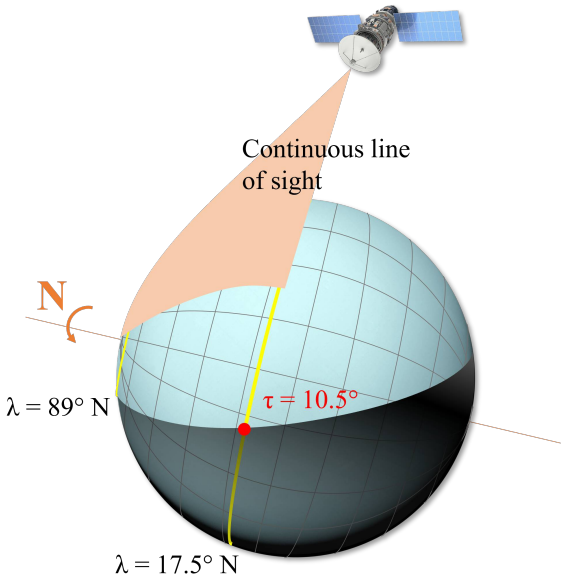

Fig. 1 The geometry of Uranus' day and night sides in 2043. The two yellow lines (λ = 17.5° N and λ = 89° N) indicate the target latitudes followed by the two gliders

Table 1 Scaled down GL-01 glider properties.

Empty mass [kg]	190	Aspect ratio	17.0
Payload mass [kg]	25	Span [m]	12.0
Wing loading [N/m^2]	224.3588	Main wing airfoil	FX62-K-153/20
Wing surface area [m^2]	8.479	Vertical and horizontal tail airfoil	FX71-L-150/25
Angle of attack range [°]	[-8.0,9.5]	α_{opt} for maximum range [°]	2.3

D. Choice of Platform

Several options were considered as atmospheric vehicles for the mission. These include conventional descent probes, propelled and un-propelled balloon-based vehicles (zero-pressure, super-pressure, and hot air balloons), cyclocopters, as well as propelled and un-propelled winged vehicles. It was determined that only descent probes and winged vehicles would be able to meet the mission's science objectives. Multiple un-propelled winged vehicles were chosen to see if such a mission could also be conducted with another type of craft than conventional descent probes.

The chosen reference vehicle is the GL-01 glider from Amalia et al. [21], with three types of control surfaces: ailerons, elevators, and a rudder. The GL-01 original design was scaled down to yield a more realistic wing loading in Uranus' atmosphere of W/S = 224.36 N/m^2. The vehicle and the reproduction of its geometry can be seen in Fig. 2. This glider was not designed with the aim of being folded to fit in a descent probe, but it is assumed that by folding its fuselage and its wings, it can fit in a descent probe such as the Mars Science Laboratory entry vehicle, which has an interior space of 3.7 m in diameter and 1.2 m in height. Concerning the vehicle's power system, if the weight of charged batteries is too large, the use of RTGs or fuel cells can be considered. Table 1 summarises the vehicles' properties. The optimal angle of attack was obtained after simulating the flight of both gliders and retrieving the angle of attack associated to their $\left(\frac{C_L}{C_D}\right)_{max}$ condition for maximum range, at each altitude's respective velocity condition. It was found that depending on the altitude, α_{opt} lied between 1.5° and 2.0°. It was then increased to 2.3° for the proper functioning of the density calculation derived from the accelerometer measurements. The glider's aerodynamic coefficients were generated with the software XFLR5 [22] for the range of parameters mentioned in Table 2. It was determined that when flying at maximum range conditions, the equatorial and polar gliders can have a time-of-flight of up to 11.57 and 12.73 Earth days, respectively.

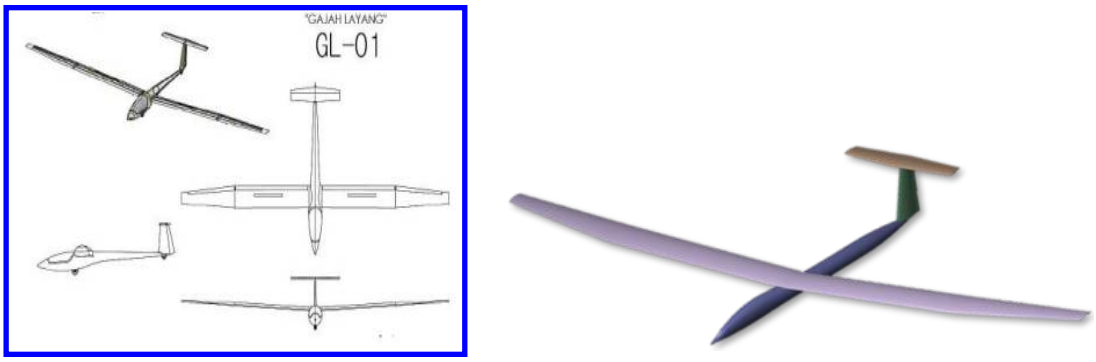

(a) Three view drawing of GL-01 glider [21]. **(b) A GL-01 glider reproduced with XFLR5, including fuselage.**

Fig. 2 GL-01 glider from literature (a) and from a reproduction made with XFLR5 (b).

Table 2 Range of parameters explored in XFLR5 to generate the vehicle's aerodynamic coefficients.

Altitude [km]	[0, -100, -200, -300, -375]
Velocity [m/s]	[9, 25, 50, 70]
Angle of attack [°]	(-8, 9.5, 0.5) for clean configuration ; (1.5, 3.5, 0.5) for deflected configuration
Aileron deflection [°]	[-25, -20, -15, -5, 0, 5, 15, 20, 25]
Rudder deflection [°]	[-25, -20, -15, -5, 0, 5, 15, 20, 25]
Elevator deflection [°]	[-30, -20, -15, -5, 0, 5, 15, 20, 30]

E. Mission Design

With a launch on May 25, 2031, the orbiter would reach Uranus 12 years later on May 17, 2043, through a purely chemical interplanetary trajectory of Venus-Earth-Earth-Jupiter fly-bys [1]. The two gliders would be released into Uranus' atmosphere by two independent descent probes targeting different latitudes: the equatorial and polar domains. The orbiter will perform the science data relay between the gliders and Earth ground stations, the Doppler wind experiment, but also the radio tracking related to navigation. It will perform a gravity-assisted capture of Uranus, release each descent probe at strategic instances making use of Uranus' fast rotation to reach the target latitudes and longitudes, and insert itself into a circular orbit.

The telecommunication between the gliders and the orbiter is inspired by the Mission Option 5 design by Hofstadter et al. [1]. It consists of an IRIS radio (X-band), an Ultra High Frequency (UHF) Solid State Power Amplifier (SSPA), and an UHF low gain antenna on-board the gliders. This design's constraints include a maximum aspect angle of 30° zenith of the gliders, and a maximum range of 100,000 km between gliders and orbiter [18]. Respecting these constraints, a geostationary orbit following the equatorial glider was found to be optimal. Respecting the planet's 17.24 h period, this places the orbiter at a maximum distance of 57,300 km and within a communication cone of 17° from the gliders.

A total data rate of 1,493 bps was estimated for the chosen scientific instrument suite, which in view of the maximum gliders' flight time of 12.73 Earth days, corresponds to 1.64 Gbits of scientific data. Considering the orbiter's uplink and downlink data rates of respectively 3 Mbps and 15,000 bps [1], 9.12 min will be needed per glider to uplink their scientific data to the orbiter, and 30.41 hr for the orbiter to transmit those data to Earth.

F. Software and GNC

The tool used and developed in this study consists of several modules describing the gliders' Environment, Aerodynamics, Flight Dynamics, Sensors, Guidance, Navigation, and Control systems. Concerning the guidance and control aspect of the mission, simple concepts were implemented to focus on navigation. The guidance system uses a reference trajectory (aerodynamic angles and heading angle) that it tries to replicate by following a set of pre-defined way-points. With the difference between the reference trajectory and the actual trajectory that the vehicle is following, the guidance system computes the necessary steering commands for the control system. It also outputs the trimming command consisting of an elevator deflection which is shown to remain quite small (between 0.048° and 0.68°). For

the purpose of this paper, a correction was applied to the bank angle for the gliders to follow their respective desired trajectories. The control module is divided into a longitudinal and a lateral controller to decouple the vehicles' symmetric and asymmetric motions, and its gains are tuned with a Linear Quadratic Regulator (LQR). We plan to simulate the vehicles' flight in 6 DoF in future work.

G. Navigation and Science

An Extended Kalman Filter (EKF) estimator is the preferred candidate for this mission and its non-linear equations of motion due to its faster convergence behaviour and lower CPU load compared to a Particle Filter (PF).

We have not implemented typical optical navigation sensors such as star sensors, Sun sensors, and navigation imagers for the navigation system's sensors due to the planet's high atmospheric opacity. Magnetometers would also be unreliable due to the poor knowledge on Uranus' magnetosphere. We considered laser ranging, where the distance between the gliders and the orbiter is deduced by measuring the time of travel between the emission and receiving of a short flash of infrared laser light. However, as the performance of laser ranging between different vehicles would present a too demanding pointing accuracy, this sensor technology was set aside as well. We thus selected sensors from the scientific instrument suite to provide input to the navigation module.

These sensors consist of an Inertial Measurement Unit (IMU), an Atmospheric Structure Instrument (ASI), and an Ultra High Frequency (UHF) transceiver. Future work will also include a Flush Air Data Sensor (FADS) [23], which is for the prupose of this work, simulated by adding white-noise errors to the gliders' real velocity values retrieved from the Flight Dynamics module. The IMU contains an accelerometer and a gyroscope to measure translational and rotational motions. The ASI consists of an accelerometer, a pressure, and a temperature sensor. It outputs static temperature, pressure, the vehicle's acceleration due to the experienced drag force, as well as the atmospheric density, from which the speed of sound and the ortho- to para-hydrogen ratio can be deduced. The modelling of this sensor is illustrated in Fig. 7. The accelerometer determines the vehicle's acceleration due to drag from the drag force retrieved from the software's Flight Dynamics module For now, the drag coefficient C_D is assumed to be determined correctly before flight, but will be updated in the final version of this study. The atmospheric density is computed from that acceleration as in Equation (1), where m is the vehicle's mass, a_D its acceleration due to the drag force, C_D its drag coefficient, S_{ref} its reference area, and V the glider's velocity relative to the atmosphere in the direction of the descent trajectory.

$$\rho = \frac{2ma_D}{C_D S_{\text{ref}} V^2} \tag{1}$$

The density measurement is then fed to the pressure sensor module where the static pressure is determined by subtracting the dynamic pressure to a database of total pressures. The temperature and pressure sensors are inspired from those presented by Ferri, F. et al. [24], where the former uses wire resistance thermometers and the latter consists of a pitot tube surrounded by a Kiel probe shielding. The temperature sensor uses two Resistance Temperature Detectors (RTDs) whose principle is based upon the Callendar-Van Dusen equation, which is used in this study to generate the instrument's data:

$$R_T = R_0 \left(1 + AT + BT^2 + (T - 100)CT^3\right) \tag{2}$$

Here, R_T represents the resistance in Ω at temperature T in °C, R_0 is the resistance at T = 0 °C, and A, B, and C are material resistance constants. For a typical platinum resistance thermometer (PT 100/15A resistor), these constants are the following: A = 3.90830 $\cdot 10^{-3}$ °C^{-1}, B = -5.77500 $\cdot 10^{-7}$ °C^{-1}, C = -4.18301 $\cdot 10^{-12}$ °C^{-1}, and R_0 = 100.0 Ω.

The UHF transceiver is used to conduct a Doppler wind experiment, yielding Doppler residuals between gliders and the orbiter, as well as between the two gliders, from which wind speeds and the presence of microwave absorbers (clouds, water, hydrogen sulfide, ammonia) can be determined. This sensor was modelled as seen in Fig. 6, where the emitting signal source is referred to as 'emitter', and the receiving one as the 'observer'. The emitter and observer's location and velocity are provided by the software's Flight Dynamics module. Equation (3) is used to calculate the pseudo range $\tilde{\rho}$ and pseudo speed $\dot{\tilde{\rho}}$ of the emitter.

$$\tilde{\boldsymbol{\rho}} = c\,(t_R - t_T) = \sqrt{(\mathbf{r_o} - \mathbf{r_g})^T(\mathbf{r_o} - \mathbf{r_g})} \qquad \text{and} \qquad \dot{\tilde{\boldsymbol{\rho}}} = c\left(1 - \frac{f_T}{f_R}\right) = \frac{(\mathbf{r_o} - \mathbf{r_g})^T(\dot{\mathbf{r}}_\mathbf{o} - \dot{\mathbf{r}}_\mathbf{g})}{\sqrt{(\mathbf{r_o} - \mathbf{r_g})^T(\dot{\mathbf{r}}_\mathbf{o} - \dot{\mathbf{r}}_\mathbf{g})}} \tag{3}$$

Here, the subscripts T and R correspond to transmitter of receiver frequency or clock time, respectively. The variables $\mathbf{r_o}$ and $\mathbf{r_g}$ correspond to the position coordinates of the orbiter and glider, respectively. Their derivatives are denoted as $\dot{\mathbf{r}}_\mathbf{o}$ and $\dot{\mathbf{r}}_\mathbf{g}$, and c is the speed of light (c = 299792.458 $\cdot 10^3$ m/s).

Table 3 Initial errors included in the IMU accelerometer.

Bias b_x, b_y, b_z	[$3{\cdot}10^{-4}$, $-3.5{\cdot}10^{-4}$, $3{\cdot}10^{-4}$]
Scale factor s_x, s_y, s_z	[$2{\cdot}10^{-4}$, $-1.7{\cdot}10^{-4}$, $2.3{\cdot}10^{-4}$]
Misalignments m_{xy}, m_{xz}, m_{yx}, m_{yz}, m_{zx}, m_{zy}	[$1{\cdot}10^{-6}$, $-1{\cdot}10^{-6}$, $-1{\cdot}10^{-6}$, $2{\cdot}10^{-6}$, $1{\cdot}10^{-6}$, $2{\cdot}10^{-6}$]

The measurements used as navigation sensor inputs thus consist of the IMU acceleration measurements, the ASI temperature and pressure measurements translated to altitude, the UHF transceiver pseudo range and pseudo range rate measurements, and the pseudo FADS velocity measurements. We have not yet finalised the modelling of the ASI and FADS instruments. Their measurements are thus simulated by adding white-noise errors to the true values retrieved from the Environment and Flight Dynamics modules. The IMU measurement frequency is set to 500 Hz, corresponding to an accumulated position error of 75.5 m and a velocity error of -0.017 m/s in nominal-state propagation at the end of flight (1,150,000 s).

The IMU bias, scaling, and misalignment instrument errors used are listed in Table 3. White-noise errors with a 1-σ value of 10^{-5} m/s^2 were also added to simulate a realistic instrument. The chosen white-noise errors associated with the ASI, UHF transceiver, and pseudo FADS measurements have 1-σ values of σ_h = 0.1 m, σ_ρ = 0.1 m, $\sigma_{\dot{\rho}}$ = 10 m/s, and σ_v = [$2{\cdot}10^{-3}$, 3.5, 1] m/s, respectively. A small value had to be attributed to the x-component of σ_v for successful convergence of the y-component of the estimated position. This value contributes to reducing the measurement noise covariance matrix **R**, as it was defined as a diagonal matrix of all instruments' measurement noises, squared. A small value of 10^{-6} was also assigned to the x-position element of the process noise covariance matrix **Q**, as part of the filter's tuning. Such small values in x-direction were necessary for the filter's y-position successful estimation due to the large Coriolis acceleration being present in the filter's y-component state propagation, which depends on the gliders' large velocity in x-direction.

III. Results

The developed EKF was used to estimate the Cartesian position in rotating frame (X_R, Y_R, Z_R), and the Cartesian velocity in rotating frame (V_{X_R}, V_{Y_R}, V_{Z_R}) of the gliders, as well as the IMU's accelerometer biases (b_x, b_y, b_z). Their estimation errors (difference between real and estimated values) are shown in Fig. 3. The curves are zoomed-in on the last 10 s of the 1,500 s test simulation, for better visibility of the error estimate (blue) and covariance bounds (red). It must be noted that the b_z estimate lies outside of the covariance bounds, which will be addressed in future work. The converged errors are in the order of 10^{-3} m for the X_R and Z_R position components, 1 m for the Y_R position component, 10^{-4} m/s for the V_{X_R} and V_{Z_R} velocity components, 10^{-2} m for the V_{Y_R} velocity component, 10^{-5} m/s^2 for the b_x and b_y IMU biases, and 10^{-3} m/s^2 for the b_z IMU bias.

The EKF was then implemented in the tool, receiving measurement inputs from the Sensor module and transforming the estimated Cartesian position and velocity variables into Spherical velocity components (velocity, flight-path angle, and heading angle), altitude, and aerodynamic angles (angle of attack, side-slip angle, and bank angle) to pass to the Guidance module. New control deflections are then generated by the Control module and implemented in the Aerodynamics and Flight Dynamics modules, thus leading to new scientific measurements from the Sensor module that are then fed to the EKF at the next time-step. It must be noted that including the filter in this process yields different ASI, UHF transceiver, and FADS measurements from the Sensor module, than the ones generated with the open-loop simulation, because of the estimated state's noise.

The tool's estimated error in Cartesian position components, Cartesian velocity components, and IMU accelerometer bias components are shown in Fig. 4, where it can be seen that the performance of the EKF decreased as neither the Y_R nor Z_R error estimates are converging within the covariance bounds. The derived error in Spherical velocity components, aerodynamic angles, and altitude are displayed in Fig. 5, where the previously-mentioned noise caused by the EKF can be seen. A solution to removing this noise is to implement a band-pass filter [25] after the EKF, to feed smooth data to the guidance module, and ultimately increase the performance of the EKF. This will be done in future work. The converged errors of all mentioned variables with the EKF being integrated in the tool are given in Table 4.

Table 4 Converged error of estimated and derived state variables from EKF, as integrated in the tool.

X_R [m]	10^{-4}	V_{X_R} [m]/s	10^{-4}	b_x [m/s^2]	10^{-7}	α [°]	10^{-3}	V [m/s]	10^{-3}	h [m]	10^{-4}
Y_R [m]	10^{1}	V_{Y_R} [m]/s	10^{-3}	b_y [m/s^2]	10^{-7}	β [°]	10^{-2}	γ [°]	10^{-3}		
Z_R [m]	10^{-1}	V_{Z_R} [m]/s	10^{-2}	b_z [m/s^2]	10^{-7}	σ [°]	10^{-4}	χ [°]	10^{-2}		

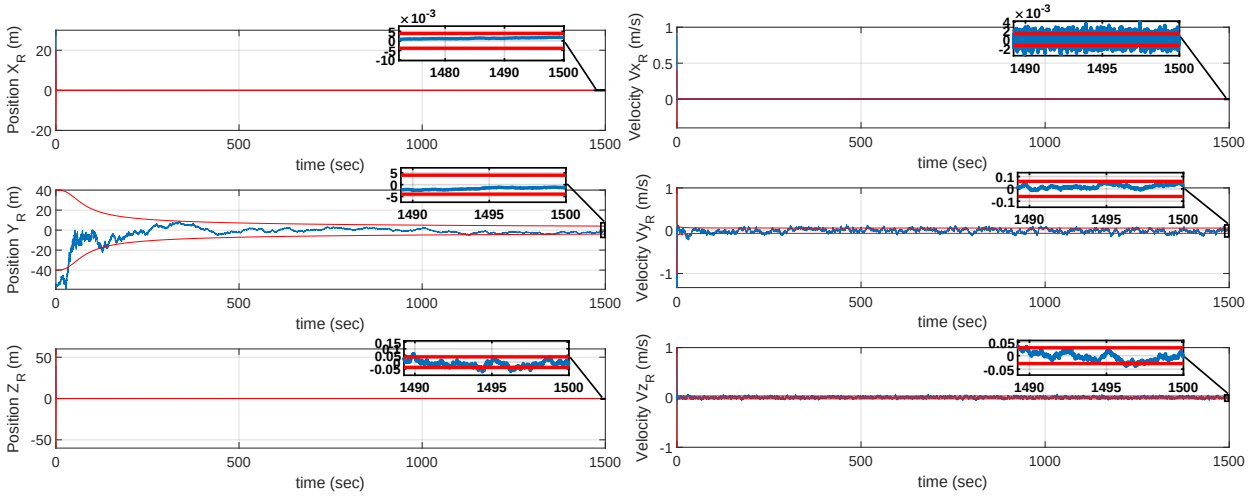

(a) Error in estimated Cartesian position in rotating frame.

(b) Error in estimated Cartesian velocity in rotating frame.

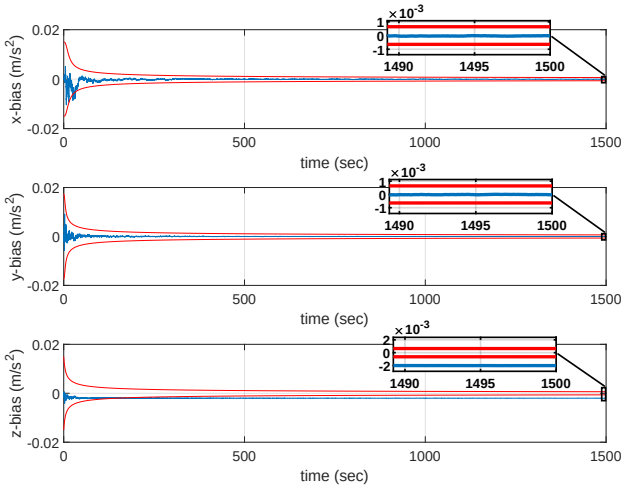

(c) Error in estimated IMU accelerometer biases.

Fig. 3 Position, velocity, and IMU accelerometer bias error estimates (blue) of the EKF filter with covariance bounds (red), as tested separately from the tool.

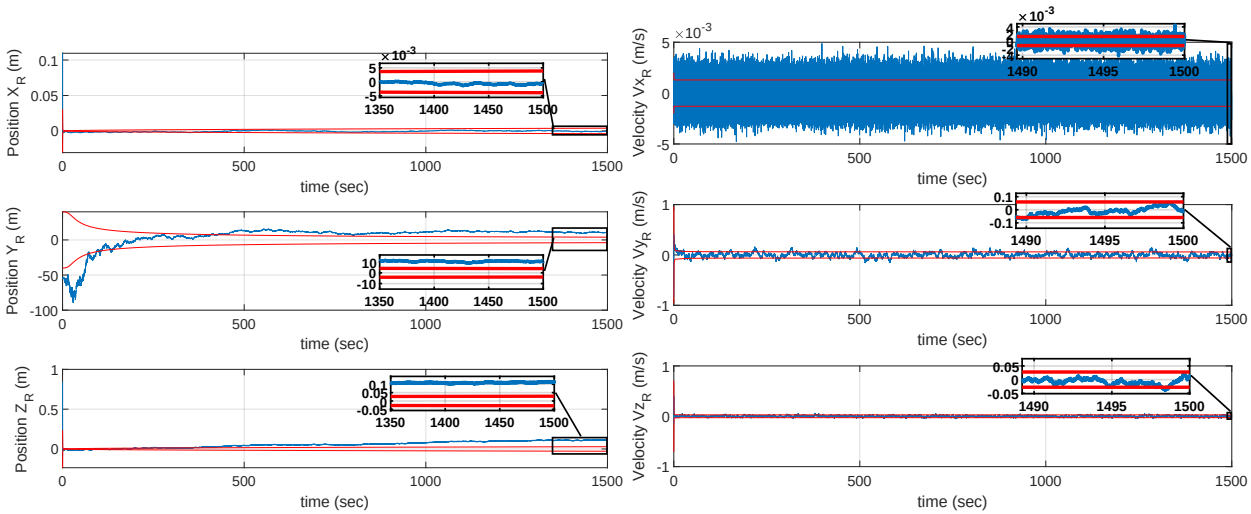

(a) Error in estimated Cartesian position in rotating frame. **(b) Error in estimated Cartesian velocity in rotating frame.**

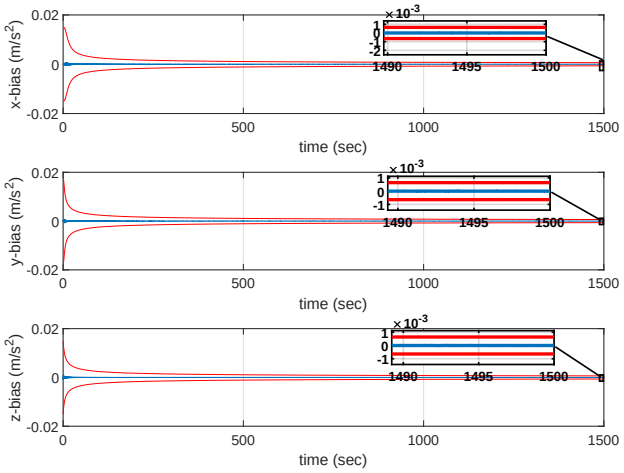

(c) Error in estimated IMU accelerometer biases.

Fig. 4 Position, velocity, and IMU accelerometer bias error estimates (blue) of EKF filter with covariance bounds (red), as integrated in the tool.

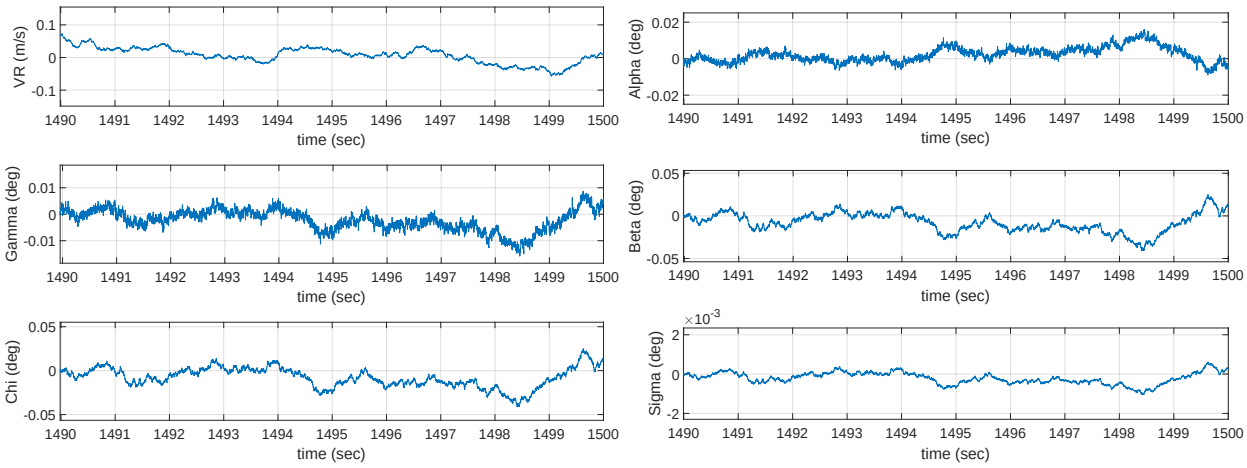

(a) Error in derived Spherical velocity.

(b) Error in derived aerodynamic angles.

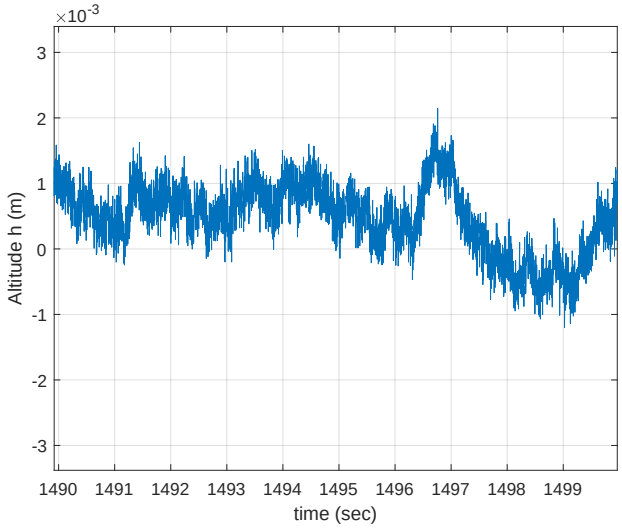

(c) Error in derived altitude.

Fig. 5 Zoomed-in Spherical velocity components, aerodynamic angles, and altitude estimates of EKF filter, as integrated in the tool.

IV. Concluding Remarks

This paper discusses the mission analysis and navigation design for an Uranus atmospheric flight of two gliders. The mission's architecture also includes an Uranus orbiter for continuous trajectory tracking and telecommunication purposes. Simulated in 3 DOF, the gliders' positions and velocity components, as well as the on-board IMU acceleration bias components are estimated with an EKF using the ASI, UHF transceiver, and FADS scientific measurements as navigation inputs. Uranus' northern equatorial domain (λ=17.5°) and polar domain (λ=89°) were selected as best target areas for measuring atmospheric properties such as noble and other gas abundances, temperature, pressure, and density profiles, and for investigating the structure and properties of the clouds.

Accurate state estimations were yielded from the implementation of the EKF, from which the following quantities were computed and passed to the guidance module: Spherical velocity components, aerodynamic angles, and altitude. The noise in the estimated state variables leads to a decrease in the navigation filter's performance, demonstrating less convergence of error estimations within the covariance bounds for the same simulation time. Future work will include the implementation of a band-pass filter to reduce the noise of the estimates and to ultimately yield better EKF performance. The IMU measurement frequency will be reduced as much as allowed by the mission requirements. The mission will also be simulated in a 6 DOF environment, including a wind model of Uranus' atmosphere. Finally, the correction made to the gliders' bank angle will also be removed through the implementation of a controller working in 6 DOF.

The significance of this work lies in the numerical proof that gliders offer a longer flight time (up to 12 Earth days) than conventional descent probes (a few hours) for the exploration of an atmosphere like Uranus'. It also paves the way for the use of payload instrument measurements as navigation input for missions where optical sensors and GNSS would not be available or impractical to use.

Appendix

Table 5 Mission Science traceability matrix.

Mission Research Question	Mission Science Objectives	Measurement Requirements	Measurement Mode							
			Mass Spectrometer	Tunable Laser Spectrometer	Helium Abundance Detector	Atmospheric Structure Instrument	NanoChem	Ultra High Frequency (UHF) Transceiver	Nephelometer	Net Flux Radiometer
How can knowledge about Uranus' current atmosphere help us understand the formation of the Ice Giants, and in a broader sense, that of the Solar System?	Tier 1	Measure the atmospheric helium abundance with an accuracy comparable to measurements made by the Galileo probe helium abundance detector at Jupiter, about 2%[a]	x		x					
		Measure the abundance of the noble gases Ne, Xe, Kr, and Ar with an accuracy close to current uncertainties in measured solar abundances, approximately 10%[b]	x							
		Measure the isotopic ratio of nitrogen $^{15}N/^{14}N$ with an accuracy of ±5%[c]	x							
		Measure the D/H ratio of hydrogen with an accuracy of ±5% or better[d]	x	x						
		Measure the helium isotope ratio $^{3}He/^{4}He$ with an accuracy at least commensurate with measurements made by the Galileo neutral mass spectrometer, ±3%[e]	x							
		Measure key noble gas isotope ratios $^{20}Ne/^{22}Ne$, $^{36}Ar/^{38}Ar$, ^{132}Xe/total Xe, ^{131}Xe/total Xe, and ^{129}Xe/total Xe with an accuracy of ±1% to enable direct comparison with other known Solar System values[c]	x							
		Measure atmospheric pressure and temperature during the atmospheric vehicle's descent with an accuracy comparable to the Galileo probe measurements at Jupiter, Pressure: 0.5%; Temperature: ±0.1° K in the upper troposphere, ±1° K at deeper levels[f]				x				
		Measure the speed of sound in the atmosphere (used to reconstruct the profile of ortho to para hydrogen along the atmospheric vehicle's descent trajectory) with an accuracy of at least 1%[g]				x				
	Tier 2A	Measure the isotope ratios of carbon $^{13}C/^{12}C$ and oxygen $^{18}O/^{17}O/^{16}O$ with accuracies of ±1%[c]	x	x						
		Measure the tropospheric abundances of CO and PH_3 with an accuracy equivalent to Jupiter and Saturn, ±5%[hi]	x	x						
		Detect and measure the abundances of other disequilibrium species in the troposphere such as AsH_3 and GeH_4 with an accuracy of ±10%[c]	x	x						
	Tier 2B	Measure the vertical (altitude) profiles of elemental abundances (relative to hydrogen) of the cosmogenically abundant species carbon, nitrogen, sulfur, and oxygen from their primary host molecules CH_4, NH_3, H_2S, and H_2O, respectively with an accuracy of ±10%, approximately equal to solar abundances measured from photospheric and meteoritic data[bc]	x	x			x	x		x
		Measure the altitude structure and properties of clouds and haze layers, including determination of the aerosol optical properties, size distributions, number/mass densities, and possibly composition							x	
		Measure the altitude profile of atmospheric dynamics along the atmospheric vehicle's descent path, including horizontal winds, waves, and convection						x		
		Measure altitude profile of the net radiative balance between solar visible insolation and upwelling thermal infrared radiation								x

[a][26] [b][27] [c][28] [d][29] [e][30] [f][31] [g][32] [h][33] [i][34]

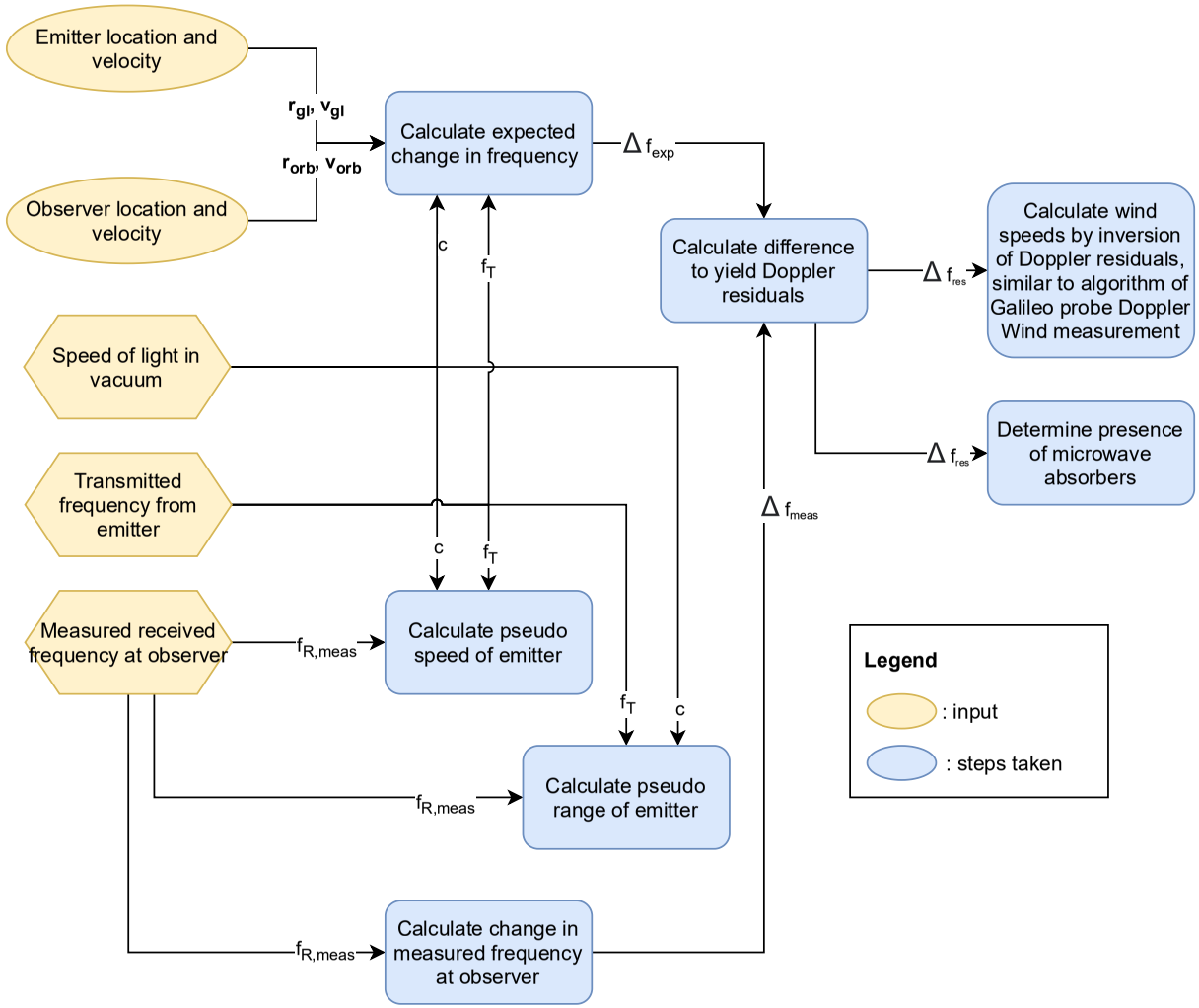

Fig. 6 Block diagram of Ultra High Frequency (UHF) transceiver.

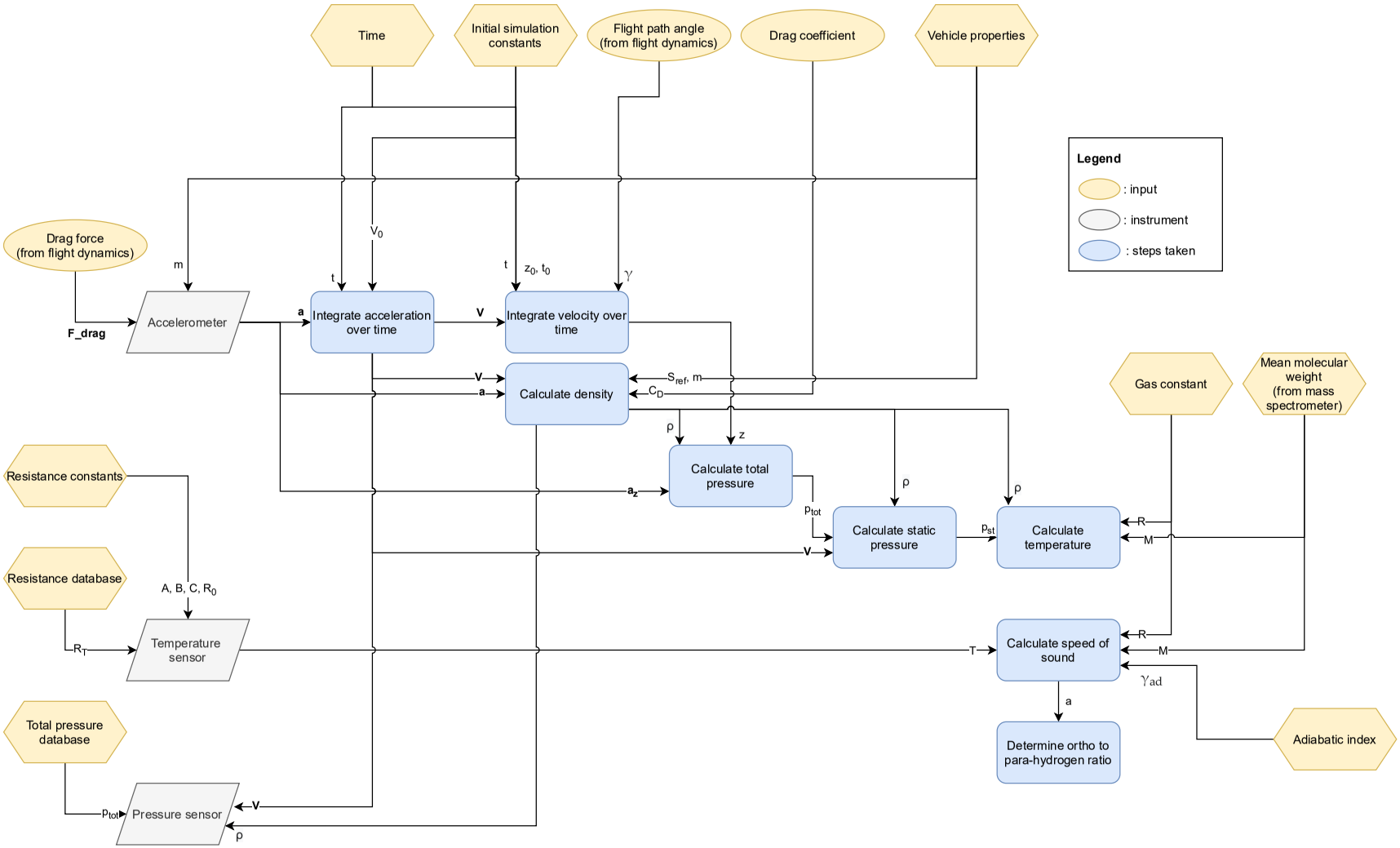

Fig. 7 Block diagram of Atmospheric Structure Instrument.

References

[1] Hofstadter, M., Simon, A., Reh, K., Elliot, J., Niebur, C., and Colangeli, L., "NASA Ice Giants Pre-Decadal Study Final Report," Tech. rep., Jet Propulsion Laboratory California Institute of Technology, Pasadena, California, Jun. 2017.

[2] Hofstadter, M. et al., "Uranus and Neptune missions: A study in advance of the next Planetary Science Decadal Survey," *Planet. Space Sci.*, Vol. 177, 2019, 104680. https://doi.org/10.1016/j.pss.2019.06.004.

[3] Fletcher, L. N. et al., "Ice Giant Systems: The scientific potential of orbital missions to Uranus and Neptune," *Planet. Space Sci.*, Vol. 191, 2020, 105030. https://doi.org/10.1016/j.pss.2020.105030.

[4] Guillot, T., "Uranus and Neptune are key to understand planets with hydrogen atmospheres," Tech. rep., Université Côte d'Azur, Laboratoire Lagrange, OCA, CNRS UMR 7293, Nice, France, Aug. 2019.

[5] Mousis, O. et al., "In situ Exploration of the Giant Planets," Tech. rep., Aix Marseille Université, CNRS, LAM, Marseille, France, Jul. 2019.

[6] Levison, H. F., and Stewart, G. R., "Remarks on Modeling the Formation of Uranus and Neptune," *Icarus*, Vol. 153, No. 1, 2001, pp. 224–228. https://doi.org/10.1006/icar.2001.6672.

[7] Gomes, R., Levison, H. F., Tsiganis, K., and Morbidelli, A., "Origin of the cataclysmic Late Heavy Bombardment period of the terrestrial planets," *Nature*, Vol. 435, No. 7041, 2005, pp. 466–469. https://doi.org/10.1038/nature03676.

[8] Morbidelli, A., Tsiganis, K., Crida, A., Levison, H. F., and Gomes, R., "Dynamics of the Giant Planets of the Solar System in the Gaseous Protoplanetary Disk and Their Relationship to the Current Orbital Architecture," *AJ*, Vol. 134, No. 5, 2007, pp. 1790–1798. https://doi.org/10.1086/521705.

[9] Batygin, K., and Brown, M. E., "Early Dynamical Evolution of the Solar System: Pinning Down the Initial Conditions of the Nice Model," *ApJ*, Vol. 716, No. 2, 2010, pp. 1323–1331. https://doi.org/10.1088/0004-637X/716/2/1323.

[10] Nesvorný, D., "Young Solar System's Fifth Giant Planet?" *ApJ*, Vol. 742, No. 2, 2011, L22. https://doi.org/10.1088/2041-8205/742/2/L22.

[11] Batygin, K., Brown, M. E., and Betts, H., "Instability-driven Dynamical Evolution Model of a Primordially Five-planet Outer Solar System," *ApJ*, Vol. 744, No. 1, 2012, L3. https://doi.org/10.1088/2041-8205/744/1/L3.

[12] Irwin, P. G. J., *Giant planets of our solar system : atmospheres compositions, and structure*, Springer, Berlin, Germany, 2003. https://doi.org/10.1007/3-540-37713-1.

[13] Helled, R., Anderson, J. D., Podolak, M., and Schubert, G., "Interior Models of Uranus and Neptune," *ApJ*, Vol. 726, No. 1, 2011, 15. https://doi.org/10.1088/0004-637X/726/1/15.

[14] Lindal, G. F., "The Atmosphere of Neptune: an Analysis of Radio Occultation Data Acquired with Voyager 2," *AJ*, Vol. 103, 1992, p. 967. https://doi.org/10.1086/116119.

[15] Hammel, H. B., Rages, K., Lockwood, G. W., Karkoschka, E., and de Pater, I., "New Measurements of the Winds of Uranus," *Icarus*, Vol. 153, No. 2, 2001, pp. 229–235. https://doi.org/10.1006/icar.2001.6689.

[16] Atkinson, D. H., Mousis, O., Spilker, T. R., and Ferri, F., "Reference Model Payload for Ice Giant Entry Probe Missions," *Space Sci. Rev.*, Vol. 216, No. 8, 2020, 120. https://doi.org/10.1007/s11214-020-00738-y.

[17] Fletcher, L. N., de Pater, I., Orton, G. S., Hofstadter, M. D., Irwin, P. G. J., Roman, M. T., and Toledo, D., "Ice Giant Circulation Patterns: Implications for Atmospheric Probes," *Space Sci. Rev.*, Vol. 216, No. 2, 2020, 21. https://doi.org/10.1007/s11214-020-00646-1.

[18] Sayanagi et al., "Small Next-Generation Atmospheric Probe (SNAP) Concept to Enable Future Multi-Probe Missions: A Case Study for Uranus," *Space Sci. Rev.*, Vol. 216, No. 4, 2020, 72. https://doi.org/10.1007/s11214-020-00686-7.

[19] Li, J., Lu, Y., Ye, Q., Cinke, M., Han, J., and Meyyappan, M., "Carbon Nanotube Sensors for Gas and Organic Vapor Detection," *Nano Letters*, Vol. 3, No. 7, 2003, p. 929–933. https://doi.org/10.1021/nl034220x.

[20] Li, J., and Lu, Y., "Carbon nanotube based chemical sensors for space and terrestrial applications," *ECS Transactions*, Vol. 19, No. 6, 2009. https://doi.org/10.1149/1.3118533.

[21] Amalia, E., Moelyadi, M. A., and Putra, C. A., "Aerodynamics characteristics of glider GL-1 based on computational fluid dynamics," Tech. rep., Institute of Technology Bandung, Bandung, Indonesia, 09 2018.

[22] Deperrois, A., "XFLR5: Analysis of foils and wings operating at low Reynolds numbers," Tech. rep., Feb. 2003.

[23] Cobleigh, B., Whitmore, S., Haering, E., Borrer, J., and Roback, V., "Flush Airdata Sensing (FADS) System Calibration Procedures and Results for Blunt Forebodies," *AIAA*, 1999. https://doi.org/10.2514/6.1999-4816.

[24] Ferri, F. et al., "The Atmospheric Structure of the Ice Giant Planets from In Situ Measurements by Entry Probes," *Space Sci. Rev.*, Vol. 216, No. 8, 2020, 118. https://doi.org/10.1007/s11214-020-00749-9.

[25] Mooij, E., "Robust Control of a Conventional Aeroelastic Launch Vehicle," *AIAA*, 2020. https://doi.org/10.2514/6.2020-1103.

[26] Von Zahn, U., Hunten, D. M., and Lehmacher, G., "Helium in Jupiter's atmosphere: Results from the Galileo probe helium interferometer experiment," *J. Geophys. Res.*, Vol. 103, No. E10, 1998, pp. 22815–22830. https://doi.org/10.1029/98JE00695.

[27] Lodders, K., Palme, H., and Gail, H. P., "Abundances of the Elements in the Solar System," *Landolt-Bornstein*, Vol. 4B, 2009, pp. 560–630. https://doi.org/10.1007/978-3-540-88055-4_34.

[28] Mousis, O. et al., "Scientific rationale for Uranus and Neptune in situ explorations," *Planet. Space Sci.*, Vol. 155, 2018, pp. 12–40. https://doi.org/10.1016/j.pss.2017.10.005.

[29] Mousis, O. et al., "The Hera Saturn entry probe mission," *Planet. Space Sci.*, Vol. 130, 2016, pp. 80–103. https://doi.org/10.1016/j.pss.2015.06.020.

[30] Mahaffy, P. R., Donahue, T. M., Atreya, S. K., Owen, T. C., and Niemann, H. B., "Galileo Probe Measurements of D/H and 3He/4He in Jupiter's Atmosphere," *Space Sci. Rev.*, Vol. 84, 1998, pp. 251–263.

[31] Seiff, A., Kirk, D. B., Knight, T. C. D., Young, R. E., Mihalov, J. D., Young, L. A., Milos, F. S., Schubert, G., Blanchard, R. C., and Atkinson, D. H., "Thermal structure of Jupiter's atmosphere near the edge of a 5-micrometer hot spot in the north equatorial belt," *J. Geophys. Res.*, Vol. 103, No. E10, 1998, pp. 22857–22889. https://doi.org/https://doi.org/10.1029/98JE01766.

[32] Banfield, D., Gierasch, P., and Dissly, R., "Planetary Descent Probes: Polarization Nephelometer and Hydrogen ortho/para Instruments," *IEEE Aerospace Conference Proceedings*, Vol. 2005, 2005, pp. 691 – 697. https://doi.org/10.1109/AERO.2005.1559359.

[33] Fletcher, L. N., Orton, G. S., Teanby, N. A., and Irwin, P. G. J., "Phosphine on Jupiter and Saturn from Cassini/CIRS," *Icarus*, Vol. 202, No. 2, 2009, pp. 543–564. https://doi.org/10.1016/j.icarus.2009.03.023.

[34] Mousis, O. et al., "Scientific rationale of Saturn's in situ exploration," *Planet. Space Sci.*, Vol. 104, 2014, pp. 29 – 47. https://doi.org/10.1016/j.pss.2014.09.014.